

# BPDA-PDA Polyimide: Synthesis, Characterizations, Aging and Semiconductor Device Passivation

S. Diaham, M.-L. Locatelli and R. Khazaka

Additional information is available at the end of the chapter

<http://dx.doi.org/10.5772/53994>

## 1. Introduction

Polyimides (PIs) are advanced polymeric materials well-known for their excellent thermal, electrical, mechanical and chemical properties [1]. PIs are particularly attractive in the microelectronics industry due to their high thermal stability ( $T_d$ ), high glass transition temperature ( $T_g$ ), low dielectric constant, high resistivity, high breakdown field, inertness to solvent, radiation resistance, easy processability, etc [2,3]. Recently, the emergence of novel wide bandgap semiconductor (SiC, GaN or Diamond) devices aiming to operate between 200 °C and 400 °C make PIs as one of the most potential organic materials for the surface secondary passivation [4]. In such a high temperature range of operation with large thermal cycling constraints imposed by both the devices and the ambient temperature, the thermo-mechanical properties of passivation PIs appear as fundamental to ensure long lifetime of the materials and reliable behaviour of the devices. For instance, Table I shows some electrical, thermal and mechanical properties of wide band gap semiconductors compared to those of silicon (Si).

	$E_g$ (eV)	$\epsilon_r$	$E_{br}$ (MV/cm)	$\lambda_{th}$ (W/m/K)	CTE (ppm/°C)
Si	1.1	11.8	0.2	150	3
GaN	2.3-3.3	9-11	1.3-3.3	80-130	5.6
SiC	2.2-3.3	10	1.2-2.4	450	4
Diamond	5.4	5.5	5-10	2000	1

$E_g$ : forbidden energy band gap;  $\epsilon_r$ : dielectric constant;  $E_{br}$ : breakdown field;  $\lambda_{th}$ : thermal conductivity; CTE: coefficient of thermal expansion.

**Table 1.** Main physical properties of wide band gap semiconductor materials at 300 K.

It is possible to observe that the semiconductor materials own a low coefficient of thermal expansion (CTE) below 6 ppm/°C. Thus, among the criteria for the PI passivation material choice, the CTE,  $T_g$  and  $T_d$  temperatures are of prior importance. Table II shows some electrical, thermal and mechanical properties of the main aromatic PIs.

The classical poly(4,4'-oxydiphenylene pyromellitimide) (PMDA-ODA) appears as not well adapted for a severe thermal cycling operation due to the strong mismatch between its CTE (30-40 ppm/°C) and the one of semiconductor materials (<6 ppm/°C). This mismatch induces strong mechanical stresses in PMDA/ODA films coated on Si wafer (29 MPa). The poly(4-4'-oxydiphenylene biphenyltetracarboximide) (BPDA-ODA), the poly(4-4'-oxydiphenylene benzophenonetetracarboximide) (BTDA-ODA), the poly(*p*-phenylene benzophenonetetracarboximide) (BTDA-PDA) and the poly(*p*-phenylene oxydiphthalimide) (ODPA-PDA) have a chemical packing which leads to similar issues on Si wafer due to large CTEs mismatching ( $\geq 28$  ppm/°C). Moreover, PMDA-ODA, BPDA-ODA, BTDA-ODA and ODPA-PDA exhibit the lowest degradation temperature values due to the degradation of the C–O–C ether bond present in the PI monomer unit [1,15,16].

	$T_g$ (°C)	$T_d$ (°C)	$\epsilon_r$	$E'$ (GPa)	TS (MPa)	Film stress on Si wafer (MPa)	CTE (ppm/°C)
PMDA-ODA	>380	586	3.4	3.0	170	29	30-40
PMDA-PDA	>450	610	3.0	12.2	296	-10 (compression)	2
BPDA-ODA	325	531	3.3	3.0	230	34	28
BPDA-PDA	>330	595	3.1	10.2	597	5	3-7
BTDA-ODA	280	554	3.0	3.0	150	40	40
BTDA-PDA	>370		2.98	7.1	248	30	35
ODPA-PDA	>370		3.0	8.1	263	42	35

$T_g$ : glass transition temperature;  $T_d$ : degradation temperature defined at 10% wt. loss;  $\epsilon_r$ : dielectric constant;  $E'$ : Young's modulus; TS: tensile strength; CTE: coefficient of thermal expansion between 50 °C and 300 °C. Film stress is given for film below 20  $\mu$ m of thickness [5-14].

**Table 2.** Thermal, electrical and mechanical properties of the main aromatic PIs.

On the contrary, PIs synthesized from pyromellitic dianhydride (PMDA) or 3,3',4,4'-biphenyltetracarboxylic dianhydride (BPDA) with *p*-phenylene diamine (PDA) in order to form PMDA-PDA and BPDA-PDA, respectively, present a higher thermal stability ( $T_d=610$  °C and 595 °C, respectively) than PIs owning C–O–C ether bonds. Moreover, both appear as better candidates for the wide band gap semiconductor passivation due to their low CTEs (2 ppm/°C and 3-7 ppm/°C, respectively). For instance, PMDA-PDA and BPDA-PDA show internal stresses of -10 MPa (compression) and 5 MPa when they are coated on Si wafers (3 ppm/°C). Thus, BPDA-PDA seems to be, as given by the main thermo-mechanical properties, the most compatible PI for SiC and GaN semiconductor passivation while PMDA-PDA should be preferred for diamond passivation.

In this chapter, a particular attention is focused on the electrical properties of unaged BPDA-PDA and their evolution during a thermal aging on Si wafers in both oxidative and inert atmospheres. A comparative aging study with higher CTE's PIs (PMDA-ODA and BPDA-ODA) is carried out in order to highlight the longer lifetime of BPDA-PDA. Prior to this, a paragraph dealing with the optimization of the thermal imidization of BPDA-PDA is reported through a simultaneous analysis of the infrared spectra and the electrical properties evolutions as a function of the imidization curing temperature. Finally, an application of BPDA-PDA to the passivation of SiC semiconductor devices will be presented through the PI on-wafer etching process and the electrical characterization of bipolar diodes at high temperature and high voltage.

## 2. Synthesis and optimization of the imidization of BPDA-PDA polyimide

The final physical properties of PIs and their integrity during aging depend strongly on the control and on the optimization of the imidization reaction (i.e. the curing process) [17,18]. This process step appears as crucial for industrial applications. Unfortunately, it is quite difficult to predict *a priori* the imidization temperature optimum which leads to the best electrical properties. Literature presents a large range of imidization temperature from 200 °C to 425 °C without always indicating if it corresponds to an optimum [6,18-23]. Moreover, these works present mainly the optimization of the imidization reaction from a chemical point of view only based on *qualitative* infrared measurements. Even if the dielectric properties are strongly linked to the PIs chemical structure, it would be more adequate to optimize the imidization reaction taking into account both the chemical structure and the dielectric properties simultaneously. Indeed, dielectric characterizations can be more sensitive than infrared measurements regarding the determination of the imidization temperature optimum. In the section 2, the results are extracted from [24].

### 2.1. Material, sample preparation and curing process

BPDA-PDA PI was purchased as a polyamic acid (PAA) solution. It was obtained through the two-steps synthesis method from its precursor monomers [25]. The PAA solution was obtained by dissolving the precursor monomers in an organic polar solvent N-methyl-2-pyrrolidone (NMP). Two different viscosity types of the PAA solution were used for controlling the thickness. To convert PAA into PI, the solution was heated up to remove NMP and to induce the imidization through the evaporation of water molecules. Figure 1 shows the synthesis steps of BPDA-PDA.

The PAA solution was spin-coated on both square stainless steel substrates (16 cm<sup>2</sup>) and highly doped 2'' Si N<sup>+</sup> wafers (<3×10<sup>-3</sup> Ω cm). PAA was first spread at 500 rpm for 10 seconds followed by a spin-cast at different rotation speeds between 2000 rpm and 4000 rpm for 30 seconds. Two successive curing steps followed the coatings. After a soft-bake (SB) at a low temperature ( $T_{SB}$ ) of 150 °C for 3 minutes on a hot-plate in air, coatings were hard-cured (HC) at a higher temperature ( $T_{HC}$ ) in a regulated oven under nitrogen atmosphere and during a time  $t_{HC}$ . In the following, the  $T_{HC}$  temperature represents the imidization

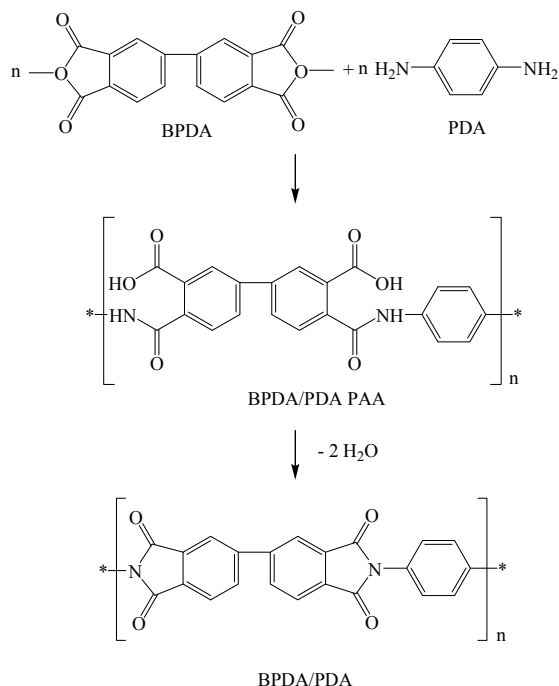


**Figure 1.** Synthesis steps of the BPDA-PDA polyimide.

temperature. The final film thicknesses have been measured using a KLA Tencor Alpha-Step IQ profilometer in a range from 1.5 to 20  $\mu\text{m}$  depending on the spin-coating parameters, the viscosity of PAA and  $T_{HC}$ . In order to perform the electrical measurements, an upper gold metallization was evaporated after imidization onto the PI film surface under vacuum ( $10^{-4}$  Pa). This metal layer was then patterned using successively a photolithography step through a selective mask and a humid gold etching to form different circular electrodes from 300  $\mu\text{m}$  to 5 mm in diameter.

The imidization cure is necessary to drive off solvent (boiling point of 202  $^{\circ}\text{C}$  for NMP), and to achieve the conversion of the PAA into PI by the formation of the imide rings. PAA coatings were hard-cured at  $T_{HC}$  in the range from 175 to 450  $^{\circ}\text{C}$  under nitrogen for a time  $t_{HC}$  of 60 minutes. The heating and cooling rates for all the samples were 2.5 and 4  $^{\circ}\text{C min}^{-1}$ , respectively.

## 2.2. Optimization of the imidization reaction

### 2.2.1. Fourier transform infrared spectroscopy (FTIR)

In order to detect the chemical bond changes during the imidization of PAA into PI, assignments of the absorption bands in FTIR spectra are necessary to identify the amide and imide peaks. The characteristic IR absorption peaks were assigned thanks to previous works

[17,26-36]. Usually, PAA spectra are compound of the N–H stretch bonds at 2900–3200  $\text{cm}^{-1}$ , the C=O carbonyl stretch from carboxylic acid at 1710–1720  $\text{cm}^{-1}$ , the symmetric carboxylate stretch bonds at 1330–1415  $\text{cm}^{-1}$ , the C=O carbonyl stretch of the amide I mode around 1665  $\text{cm}^{-1}$ , the 1540–1565  $\text{cm}^{-1}$  amide II mode and the 1240–1270  $\text{cm}^{-1}$  band due to the C–O–C ether aromatic stretch (if present in the monomer).

After the conversion reaction, the absence of the absorption bands near 1550  $\text{cm}^{-1}$  (amide II) and 1665  $\text{cm}^{-1}$  (amide I) indicates that PAA has been converted into PI. Simultaneously, this is confirmed by the occurrence of the C=O stretch (imide I) peaks at 1770–1780  $\text{cm}^{-1}$  (symmetric) and 1720–1740  $\text{cm}^{-1}$  (asymmetric), the typical C–N stretch (imide II) peak around 1380  $\text{cm}^{-1}$ , the C–H bend (imide III) and C=O bend (imide IV) absorption bands respectively in the ranges of 1070–1140  $\text{cm}^{-1}$  and of 720–740  $\text{cm}^{-1}$ . The presence in PI films of a large absorption band between 2900 and 3100  $\text{cm}^{-1}$  is associated to the C–H stretch bonds. Finally, the measurements may highlight the occurrence of a shoulder on the asymmetric C=O stretch bonds at 1710  $\text{cm}^{-1}$  which corresponds to the out-of-plane optical response of the imide I conformation [37].

Figure 2 shows FTIR spectra of both PAA coatings after the SB at 150 °C and PI films after a HC at 250 °C. Spectra have been normalized to the classical C=C absorption band appearing at 1518  $\text{cm}^{-1}$ . The spectrum performed after the SB shows the typical absorption bands of PAA coatings. The large absorption band observed between 2300 and 3400  $\text{cm}^{-1}$  corresponds to the N–H stretch vibration modes, the C–H stretch bonds and the O–H stretch bonds present in both the PAA and NMP solvent. The FTIR spectrum of PI films already shows the typical completion of the imidization reaction with the presence of the four absorption bands from the imide rings. They occur at 1775/1734  $\text{cm}^{-1}$  (imide I), 1371  $\text{cm}^{-1}$  (imide II), 1124/1080  $\text{cm}^{-1}$  (imide III) and 737  $\text{cm}^{-1}$  (imide IV). Moreover, it is possible to observe the large absorption band induced by the C–H stretch vibration modes between 2600 and 3100  $\text{cm}^{-1}$ . At 1415  $\text{cm}^{-1}$ , a shoulder appears near the C–N stretch peak. This absorption band could be attributed to symmetric stretch of carboxylate ion  $\text{COO}^-$ . The carboxylic acid groups present in PAA appear through the O–H stretching bonds at 3400  $\text{cm}^{-1}$  but free

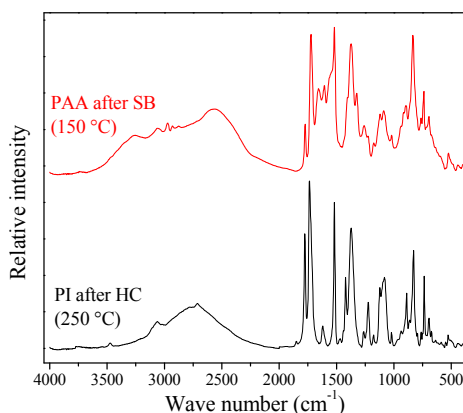


**Figure 2.** FTIR spectra of BPDA-PDA PAA coatings and PI films (thickness: 1.5  $\mu\text{m}$ ). Taken from [24].

carboxylic acid groups can be deprotonated by the weak amine base [36]. Consequently, COO<sup>-</sup> carboxylate ions are usually also present in PIs exhibiting two peaks around 1606 and 1415 cm<sup>-1</sup>. This could explain the release of mobile H<sup>+</sup> protons (from COOH) responsible of electrical conduction in PI [38].

FTIR measurements have been performed for different imidization temperatures  $T_{HC}$  to determine the completion of the imidization reaction of the PI films. This analysis rests on the absorption peak magnitude changes in the functional groups or in the characteristic linkages during the reaction. Figure 3a shows the changes in FTIR spectra of BPDA-PDA for different imidization temperatures. When  $T_{HC}$  increases, a general increase in all the absorption peaks is observed. This suggests that residual PAA monomers continue to be converted into PI. This evolution is stabilized after exposure to temperature above 350 °C.

To study the imidization kinetics of PI films, the peak of aromatic ring (C=C) stretching around 1500 cm<sup>-1</sup> is chosen as a reference and the peak height method is adopted to calculate the amount of the appearing imide groups formed. The degree of imidization (DOI) is thus defined by comparing the intensity of an imide absorption peak normalized to the intensity of the C=C reference band and is given by [27]:

$$DOI_{T_{HC}} = \frac{(A/A^*)_{T_{HC}}}{(A/A^*)_i} \quad (1)$$

where  $A^*$  is the peak height of the C=C reference band at 1518 cm<sup>-1</sup> and  $A$  is the imide peak height (i.e. 1775, 1732, 1420, 1371, 1080 and 737 cm<sup>-1</sup>). Subscripts  $i$  and  $T_{HC}$  indicate the reaction at the initial and a given imidization temperature, respectively.

Figure 3b shows the extent of imidization of the main bonds of BPDA-PDA versus the imidization temperature. Most of the imidization reaction takes place rapidly with a

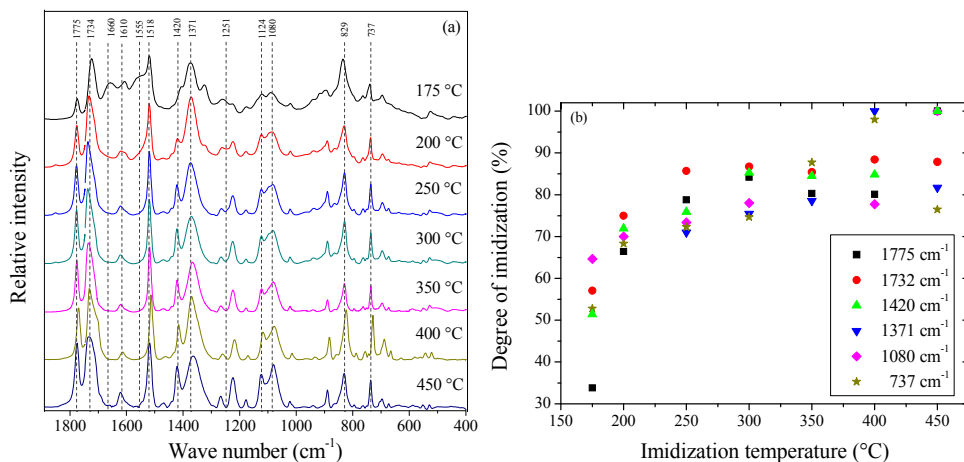


**Figure 3.** (a) FTIR spectra of BPDA-PDA for different  $T_{HC}$  (thickness: 1.5  $\mu\text{m}$ ). (b) Degree of imidization for the main absorption bands versus the imidization temperature. Taken from [24].

conversion rate as high as 70-85% at 250 °C and still continues slightly up to 400 °C as shown through the increase in the magnitude of the imide bands. However, it is difficult to detect the optimum imidization temperature (i.e. the highest magnitude) to not exceed in order to preserve PI from degradation. For instance at 450 °C, the imide II and IV absorption bands decrease of 20% and 10% respectively showing the initiation of a desimidization of the structure. Therefore, the use of complementary electrical measurements as a probe of the imidization advancement can allow obtaining a higher accuracy regarding the optimal temperature of the curing.

### 2.2.2. Electrical properties

As for the DOI, the electrical properties strongly depend on the imidization temperature. Changes in the electrical conductivity, dielectric properties or in the dielectric breakdown field of the PI films can be used to determine precisely the optimal imidization temperature. Larger the DOI is, better the electrical properties are expected due to a lower impurities amount in the PI films.

Current-Field ( $j$ - $F$ ) measurements up to 1 MV/cm show that, as soon as the low field range (10 kV/cm), the minimum of the dc conductivity ( $\sigma_{DC}$ , evaluated from the  $j$ - $F$  curves) is obtained for an imidization cure of 400 °C (as seen in Figure 4a). Whereas the  $\sigma_{DC}$  values are poorly dispersed between  $10^{-17}$  and  $10^{-16} \Omega^{-1} \text{cm}^{-1}$  up to 200 kV/cm whatever  $T_{HC}$ , the measurements show a strong divergence at high fields from 400 kV/cm. In this field range, the dc conductivity of BPDA-PDA increases much more for imidization curings at 350 °C and 450 °C (as seen in Figure 4a). Thus, the highest insulation quality (i.e. the lowest  $\sigma_{DC}$ ) has been obtained for the films imidized at 400 °C. For  $T_{HC}=400$  °C, the charges density and/or their mobility seem to be strongly reduced with this optimal imidization temperature. Usually, the electrical conduction in PI films is related to the motion of  $\text{H}^+$  protons coming from unreacted PAA [38]. This is in likelihood agreement with the evolution of the COO-band intensity which reaches its lowest magnitude at 400 °C before it increases again

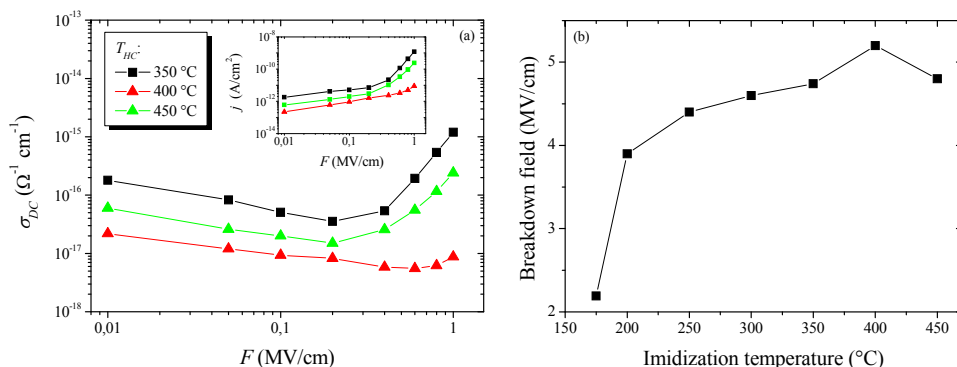


**Figure 4.** (a) Volume conductivity versus electric field of BPDA-PDA for different  $T_{HC}$  (thickness: 1.5  $\mu\text{m}$ ). (b) Breakdown field versus the imidization temperature (mean of 20 tested samples). Measurements performed at room temperature. Taken from [24].

at 450 °C (as seen in Figure 3b). This observation is emphasized by the changes in the dielectric breakdown field ( $E_{BR}$ ) as a function of the imidization temperature (as seen in Figure 4b). Indeed, after a continuous increase in  $E_{BR}$  up to  $T_{HC}=400$  °C, a sudden decrease in its magnitude when  $T_{HC}$  is raised up to 450 °C is observed. The degradation of the electrical properties above  $T_{HC}=400$  °C appears as a consequence of desimidization (i.e. the decrease in the imide bands) of BPDA-PDA structure leading to the release of free mobile charges in the bulk.

### 3. Thickness influence on the structural and dielectric properties of BPDA-PDA polyimide

#### 3.1. Influence on the chemical structure

The influence of the thickness of PI films on the chemical structure is rarely investigated. Figure 5 shows FTIR spectra of BPDA-PDA imidized at 400 °C for different film thicknesses. As represented by the downward arrows, one can observe that the quantity and the intensity of the bands corresponding to the amide bonds increase when increasing the film thickness. Hence, for higher film thicknesses, the conversion rate of PAA into PI is strongly affected either due to a bad diffusion of the temperature within the medium of the coating bulk during the curing process (presence of unreacted PAA) or due to a higher difficulty to remove by-products such as solvent and water molecules inherent in the imidization reaction. Unfortunately, this issue cannot be solved by higher temperatures or longer curings because in this range the desimidization of PI starts. Consequently, all these remaining impurities can act as ionizable centers supplying free mobile charges.

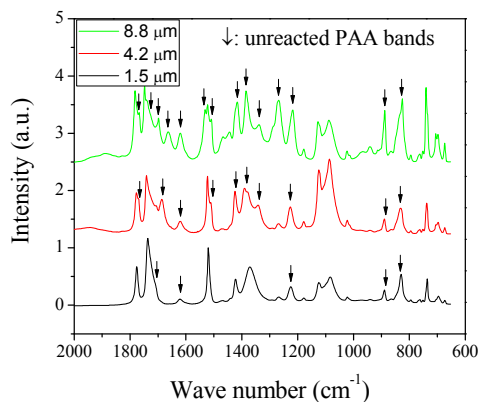


**Figure 5.** FTIR spectra of 400 °C-imidized BPDA-PDA for different film thicknesses.

#### 3.2. Influence on the electrical properties

Whereas such a phenomenon can be negligible for low temperature applications (< 150 °C) because of the low mobility of free charges, this can be more influential at high temperature



(>200 °C). Figure 6a shows the temperature dependence of the dc conductivity of BPDA-PDA between 200 °C and 350 °C for thicknesses from 1.5 μm up to 20 μm. At 200 °C, the dc conductivity is one order of magnitude higher for the thickest films compared to the one of the thinnest films. In comparison at 300 °C, the dc conductivity is two orders of magnitude higher for the thickest films than for the thinnest ones. The fact that the low field dc conductivity is thickness-dependent, particularly in the high temperature range, is directly related to the presence into BPDA-PDA of unreacted PAA impurities for which temperature supplies sufficient energy to the free charges to become mobile.

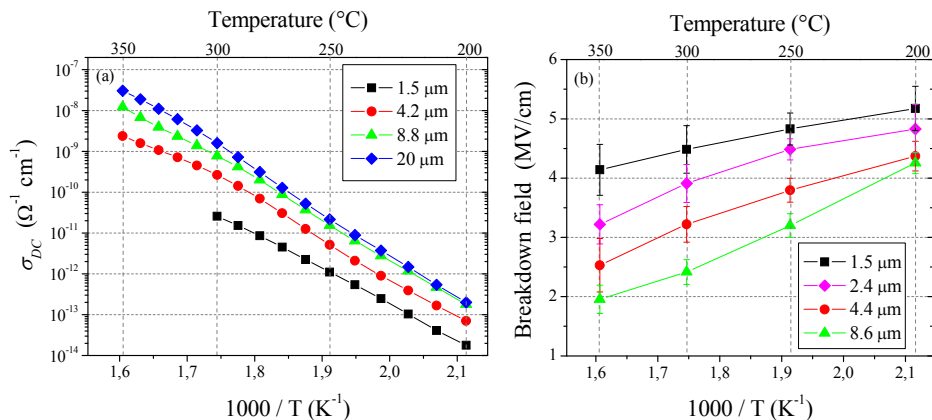


**Figure 6.** Temperature dependence of the dc conductivity (a) and breakdown field (b) of BPDA-PDA for different film thicknesses.

Figure 6b shows the temperature dependence of the dielectric strength of BPDA-PDA between 200 °C and 350 °C for thicknesses from 1.5 μm up to 8.6 μm. Same findings can be done in this high electric field region. The larger presence of PAA impurities in the thickest films leads to substantially decrease the dielectric breakdown field of 15% at 200 °C (compared to thinnest films) and of 55% at 350 °C. In these thick films, the earlier breakdown event could be explained by a prematured Joule effect occurring when a higher conduction current magnitude happens across the film during the voltage raising. Thus, the breakdown channel appears for lower applied electric fields.

#### 4. Thermal aging of BPDA-PDA polyimide

The effect of long time aging of polyimide at high temperature (>200 °C) and in oxidative environment on the mechanical properties [39], weight loss [40,41], and chemical properties [42,43], was widely investigated for thick polyimide matrix composites (1 mm thick) used in high temperature aerospace applications. It was found that while thermal degradation occurred throughout the material, the oxidative degradation occurs mainly within a thin surface layer where oxygen diffuses into the material. Few papers discussed the effect of thermal aging on the electrical properties of PIs and this is always for thick and freestanding films [44,45]. Consequently, an overall understanding of the thermo-oxidative aging

mechanisms (for PI thickness  $<20\ \mu\text{m}$ ) and their effects on the electrical properties are still lacking.

All the measurements presented below were performed on PI films deposited on highly doped  $\text{N}^{++}$  cleaned silicon wafers (resistivity  $< 3 \times 10^{-3}\ \Omega\ \text{cm}$ ) and aged at high temperature. The time at the beginning of the aging is noted as  $t_0$ . At scheduled times, a part of the specimens were removed from the oven and subjected to non-destructive and destructive tests. The thicknesses noted in the text and labels refer to the initial ones measured at  $t_0$ .

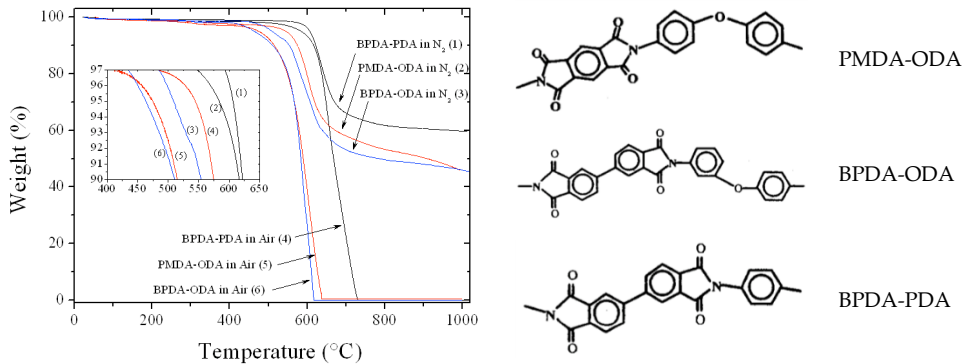


**Figure 7.** Dynamical TGA of PMDA-ODA, BPDA-ODA and BPDA-PDA in air and nitrogen.

#### 4.1. Thermal stability of PIs

For PIs, it has been shown that the increase in the number of benzene rings contributes to an increase in the degradation temperature [1]. However, the degradation temperature can be also affected by the presence of low thermo-stable bonds in the macromolecular structure. For instance, even if BPDA-PDA and PMDA-ODA (Kapton-type) own the same number of benzene rings (i.e. three in elementary monomer backbone), the absence of the C—O—C ether group in the case of BPDA-PDA allows increasing  $T_d$  (defined at 10% wt. loss) of 48 °C in nitrogen and 100 °C in air in comparison to  $T_d$  of PMDA-ODA (see Figure 7). Moreover, if the diamine ODA is replaced by PDA in BPDA-based PIs,  $T_d$  increases of 68 °C in nitrogen and 105 °C in air. Indeed, this is due to the lower thermal stability of the ether bonds inducing earlier degradations than the rest of the structure [1,44].

#### 4.2. Thermal aging in inert atmosphere

Figure 8 shows the evolution of the FTIR spectrum of BPDA-PDA before and after an aging at 300 °C in nitrogen during 1000 h and the evolution of the film thickness and the related breakdown field during this aging. One can notice that at this temperature in inert atmosphere, no change in the vibration bonds is remarkable even after a long period of aging. This is in agreement with a good stability of both the film thickness and the high field dielectric properties.

Moreover, a similar observation were done for aging at higher temperature. Indeed, up to  $T_g$  at 360 °C in nitrogen, both a stability of the chemical structure and the breakdown field were observed during 1000 h. This concludes that BPDA-PDA does not evolved up to 360 °C in inert atmosphere.

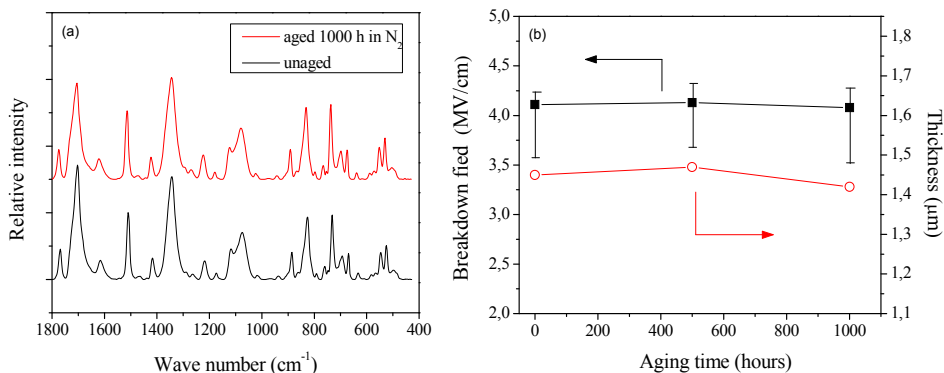


**Figure 8.** (a) FTIR spectra before and after aging in  $N_2$  at 300 °C and (b) breakdown field and thickness during aging for 1.5  $\mu\text{m}$ -thick BPDA-PDA films. The breakdown field is measured at 300 °C.

### 4.3. Thermal aging below $T_g$ in oxidative atmosphere

The aging effects up to 5000 h at 300 °C in air on different properties of BPDA-PDA were measured on three different initial thicknesses varying from 1.5  $\mu\text{m}$  to 8  $\mu\text{m}$ . For comparison, a same aging was performed on BPDA-ODA, with a glass transition  $T_g$  of 330 °C, up to 1000 h.

The chemical structure variation was measured by FTIR and the spectra of the 4.2  $\mu\text{m}$ -thick film is presented in Figure 9a. A quasi-stabilisation of almost all the peaks can be revealed during 5000 h specially the imide ones (see Figure 9b). However, an increase in the peak localized at 1212  $\text{cm}^{-1}$  related to the asymmetric vibration of the C-O-C band can be observed. This can indicate the occurrence of additional oxidation of the unreacted polyamic acid, which was not completely imidized during the curing cycle.

On the contrary, for BPDA-ODA films (see Figure 9c and 9d), the same aging at 300 °C during 1000 h shows as soon as the first 200 h a strong decrease in all the main vibration bonds. Consequently, such an aging affects the chemical integrity of the chemical backbone and the physical properties would be modified.

If we look at the film thicknesses, the BPDA-PDA films do not show any thickness variation during 5000 h of aging, indicating that neither densification nor degradation occurred. On the other hand, the BPDA-ODA films loose more than 50% of their initial thickness after 1000 h of aging, reflecting the strong degradation in this case.

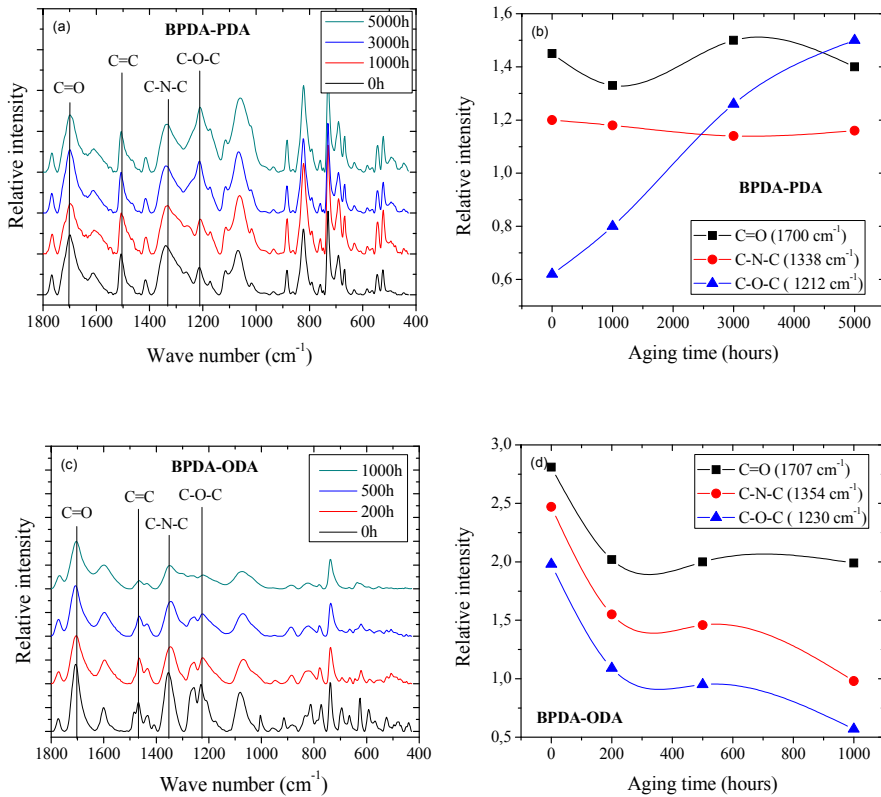


**Figure 9.** FTIR spectra during the aging in air at 300 °C for 4.2 μm-thick BPDA-PDA and 13.7 μm-thick BPDA-ODA films.

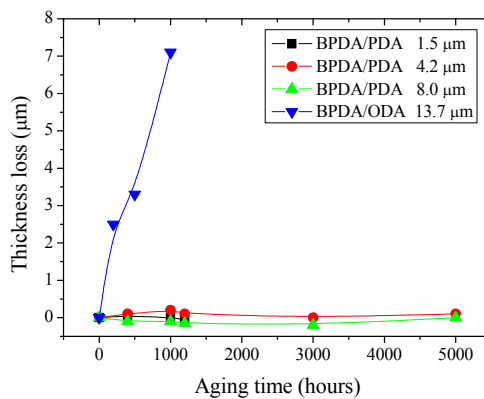


**Figure 10.** Thickness loss during the aging at 300 °C in air for three initial thicknesses of BPDA-PDA and a 13.7 μm initial thickness of BPDA-ODA.

The effect of the aging under air atmosphere on the breakdown field and low field dielectric properties measured at the aging temperatures, for the BPDA-PDA and BPDA-ODA films, are now presented and discussed. The breakdown field, performed by polarizing positively the gold electrode, for different initial BPDA-PDA thicknesses and one BPDA-ODA thickness are presented in Figure 11. Whereas a stabilization of the breakdown field during the 5000 h aging is observed for the BPDA-PDA films, a continuous decrease is observed for the BPDA-ODA films. This invariance of the breakdown field of BPDA-PDA is in good agreement with the good stability of FTIR spectra during aging. On the contrary, the strong decrease in the breakdown field of BPDA-ODA after only 1000 h highlights the progressive and fast degradation of the imide bonds in this kind of PIs.

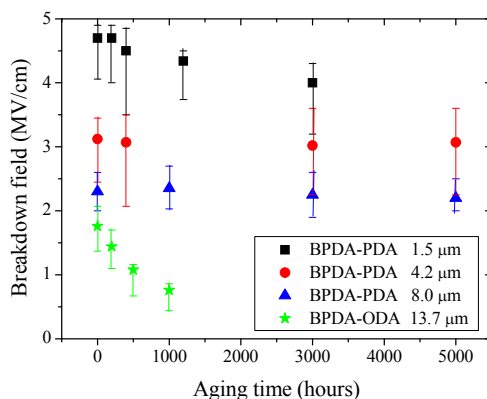


**Figure 11.** Breakdown field during the aging at 300 °C in air for three different thicknesses of BPDA-PDA and the 13.7  $\mu\text{m}$ -thick films of BPDA-ODA. The breakdown field is measured at 300 °C.

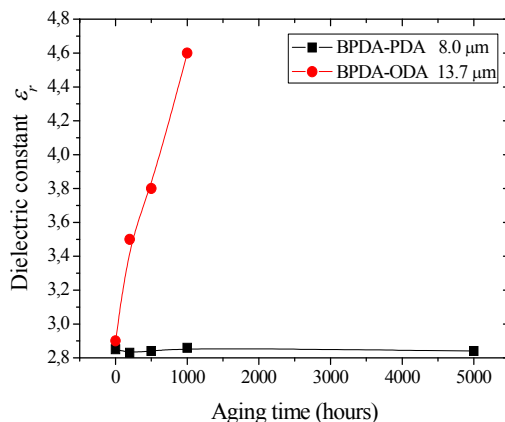


**Figure 12.** Dielectric constant measured at 300 °C and at 1 kHz during the aging for BPDA-PDA and BPDA-ODA films.

The dielectric constant  $\epsilon_r$  measured at 300 °C and at a frequency of 1 kHz during the aging is illustrated in Figure 12. Here also, while an invariance in the  $\epsilon_r$  values can be observed for the BPDA-PDA films, a huge increase in  $\epsilon_r$  is observed during the aging for the BPDA-ODA films. This increase could be attributed to the chain breakage, already observed on the FTIR spectra, leading to the formation of polar groups in the dielectric bulk. Different authors observed such behavior during the aging of PIs films at high temperature in air [45, 46]. The degradation of BPDA-ODA films is also reflected on the DC conductivity values (not presented here) that increase from  $2 \times 10^{-12}$  to  $4 \times 10^{-11} \Omega^{-1} \text{ cm}^{-1}$  after 1000 h of aging.

#### 4.4. Thermal aging above $T_g$ in oxidative atmosphere

In order to check the stability of BPDA-PDA films at higher temperatures, aging has been performed at different temperatures above  $T_g$ . Figure 13 shows a comparison of the evolution of FTIR spectra of BPDA-PDA and PMDA-ODA during an accelerated aging at 400 °C during 200 minutes in air. It can easily be observed that BPDA-PDA remain stable after aging while PMDA-ODA is strongly degraded and even if the latter owns a comparable thermal stability and a higher  $T_g$  (see Table II).

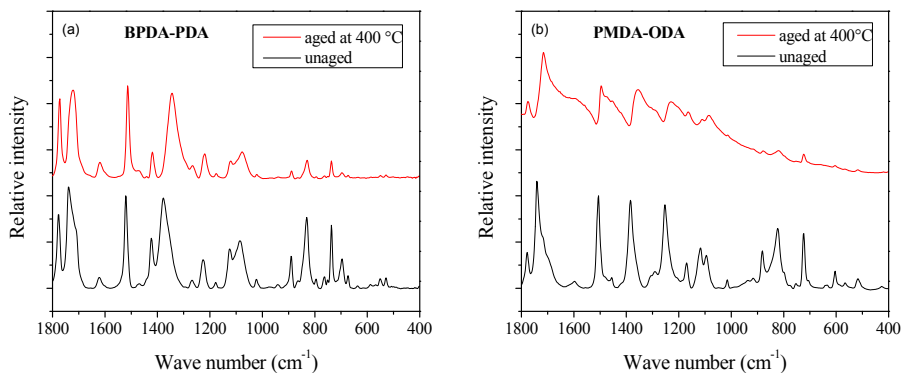


**Figure 13.** FTIR spectra before and after aging at 400 °C in air for 200 minutes for BPDA-PDA and PMDA-ODA films.

BPDA-PDA films 4.2  $\mu\text{m}$ -thick were aged in air at 360 °C during 800 h. The FTIR spectrum does not show any variation in the imide bonds during this aging period (not shown here) indicating that the bulk of the material is not affected by the aging. Here also, the measured relative permittivity at 1 kHz remains constant with a value of 2.8 during all the aging period (not shown here), indicating that no additional polar groups are formed during the aging. In contrast the film thickness and the breakdown field measured at 300 °C, present a slight continuous decrease during the aging as illustrated in Figure 14. After 800 h a breakdown field decrease of about 50 % while a thickness reduction of 14% can be measured. During this aging, an increase in the surface roughness of BPDA-PDA and the formation of craters were observed (not shown here). They can cause local field

intensification and assist the dielectric breakdown mechanism. Such a surface state degradation can explain the breakdown field decrease during the aging. So, it is believed that the observed degradations are related to the oxygen presence since no variation occurs during aging at the same temperature but in inert gas. Thus, BPDA-PDA is attacked at the outer layer face exposed to oxygen.

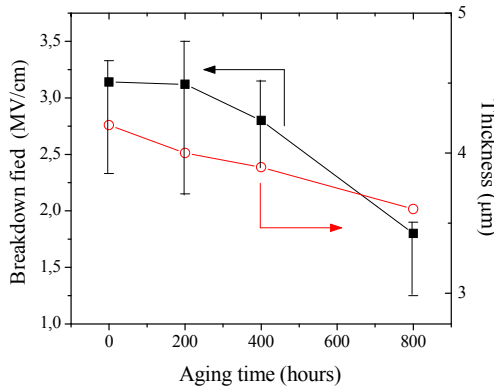


**Figure 14.** Breakdown field and thickness for 4.2  $\mu\text{m}$ -thick BPDA-PDA films during aging at 360 °C in air. The breakdown field is measured at 300 °C.

All these results lead to show that BPDA-PDA is a reliable kind of PIs in order to passivate wide band gap semiconductor devices up to 360 °C during extremely long duration in inert atmosphere without any remarkable properties degradation.

## 5. Secondary passivation of SiC bipolar diodes with BPDA-PDA polyimide

The secondary passivation is the last fabrication step, at the wafer level, of a semiconductor device. It aims to reinforce the die protection against mechanical aggressions, chemical contamination, and surface electric flashover under blocking voltage operation. Note that after the wafer dicing and die packaging, a complementary insulating environment (moulding case, silicone gel, ...), may be required over the device depending on the maximal voltage rating, in order to avoid electrical arcing in air during operation. Coming back at the wafer level, the component secondary passivation fabrication step consists in two main phases: the first one corresponds to the wafer PI coating, the second one corresponds to the PI film etching at the component metal electrode areas, in order to allow ulterior electrical contacting.

The feasibility of using BPDA-PDA polyimide for the passivation of high voltage silicon carbide bipolar diodes has been studied [47]. As BPDA-PDA material is not photosensitive and not removable using wet etching, its local etching requires applying a plasma process through a previously deposited metal mask. The following sections will first present the aimed diode structure and the used BPDA-PDA coating and etching processes. Then, the

component electrical characterizations will be reported. The results of this paragraph are extracted from [47].

### 5.1. Diodes fabrication, passivation process and plasma etching

4H-SiC PiN diodes were realized on a 2''-SiC wafer in a 60  $\mu\text{m}$ -thick  $\text{N}^-$  epilayer ( $N_D=8.4\times 10^{14} \text{ cm}^{-3}$ ), with a Al-implanted  $\text{P}^+$  emitter ( $N_E=10^{19} \text{ cm}^{-3}$ ), and a Al-implanted junction termination extension (JTE) periphery (with  $L_{\text{JTE}}\geq 125 \mu\text{m}$ , an implanted-Al dose of  $1.1\times 10^{13} \text{ cm}^{-2}$ , assuming a 80% electrical activation [48]). The common post-implantation annealing was performed at 1650  $^\circ\text{C}$  for 30 minutes in Ar. The theoretical breakdown voltage of these PiN JTE diodes, derived from ionization integral calculations realized by numerical 2D-simulations, taking into account the Konstantinov's ionization coefficients [49], is equal to 7.8 kV for the  $0.9\times 10^{13} \text{ cm}^{-2}$  JTE doping dose assumed. The primary passivation layer is a 40 nm-thick thermal  $\text{SiO}_2$  oxide grown by dry oxidation at 1150  $^\circ\text{C}$  for 2 h followed by a post oxidation annealing at 1150  $^\circ\text{C}$  for 1 h in  $\text{N}_2$ . Then, after the  $\text{SiO}_2$  layer selective opening, a first Ni/Al thin metallization was deposited, patterned and annealed to realize the low resistive ohmic contact to the diode  $\text{P}^+$  emitter areas (of 250  $\mu\text{m}$  to 1 mm in diameter). Then a 2  $\mu\text{m}$ -thick Al metallisation was evaporated and patterned as well to obtain thick anode plots. Note that some electrical tests at that stage were performed on the wafer outside the clean room.

Then, the second passivation layer has been realized with the spin-coated BPDA-PDA through a multi-layer (3 layers) coating process onto the wafer. In order to reinforce the adhesion with the primary passivation layer, an adhesion promottor (containing silane groups) was first spin-cast onto the wafer at 3000 rpm. A first layer of BPDA-PDA PAA solution was spin-coated at 500 rpm followed by a rotation speed at 3000 rpm. The wafer was consecutively baked at 100  $^\circ\text{C}$  for 1 minute and 175  $^\circ\text{C}$  for 3 minutes on a hot plate. A second and a third BPDA-PDA PAA layers were coated with the same process in order to increase the passivation layer thickness. The wafer was finally hard cured (*apart from the clean room*) in a regulated oven under nitrogen atmosphere at 200  $^\circ\text{C}$  for 15 minutes (to drive off NMP solvent) followed by a slight raising slope of 2  $^\circ\text{C min}^{-1}$  up to 400  $^\circ\text{C}$  for 1h. After the imidization, the wafer was cooled down with a low slope of -4  $^\circ\text{C min}^{-1}$ . The resulting BPDA-PDA thickness onto the wafer was 4  $\mu\text{m}$ .

Before the etching, a mask metallic layer of 300 nm was evaporated into vacuum onto the BPDA-PDA passivation layer. The metallic layer was opened (metal etch) just above the SiC diode anodes using the photolithography technique. Plasma etching of the unmasked BPDA-PDA areas was performed into a plasma reactor containing a 100%  $\text{O}_2$  atmosphere at pressure of 1 mTorr. The injected micro-wave electrical power was 600 W. An auto-polarization voltage of -84 V was applied between the plasma electrodes. The incident RF power was 70 W while the reflected power was negligible (around 3 W). The wafer was placed onto the ground electrode of the reactor which was cooled with water to maintain the temperature of the wafer around 10  $^\circ\text{C}$ . The etching was performed during 20 minutes by short steps of 5 minutes long in order to avoid an increase in the temperature of the wafer



and until the total removing of exposed BPDA-PDA areas. Figure 15 shows optical and SEM images of the upper electrode of a SiC diode after the plasma etching of BPDA-PDA.

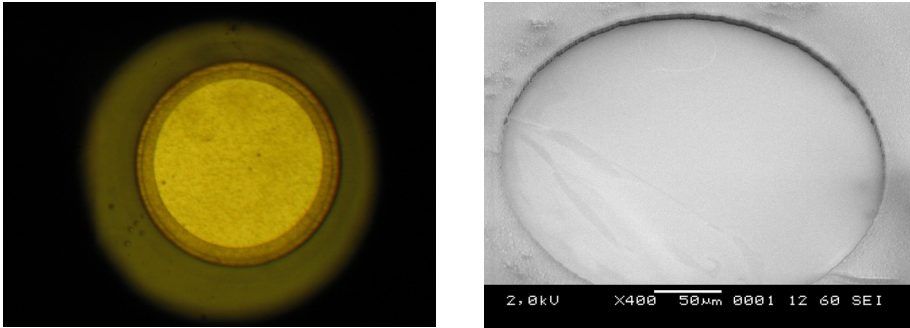


**Figure 15.** (a) Optical microscope image and (b) SEM image of the topside view of a SiC diode after the etching of BPDA-PDA secondary passivation.

## 5.2. Electrical characterizations of BPDA-PDA passivated SiC bipolar diodes

The diode forward and reverse current *vs.* voltage  $I(V)$  characteristics were measured using a Keithley 2410 source meter, at low levels (less than  $1 \text{ A/cm}^2$  forward current density and  $-600 \text{ V}$  reverse voltage) to avoid stressing the devices. These preliminary measurements were performed at different temperatures (the wafer sample being attached to a heating chuck), and in air ambient at low pressure ( $10^{-3} \text{ mbar}$ ). Then the diodes exhibiting the lowest reverse currents (less than  $10^{-6} \text{ A}$  up to  $-600 \text{ V}$ ) were selected for high reverse voltage measurements, performed in a perfluoropolyether oil (PFPE Galden® fluid, with a high dielectric strength around  $16 \text{ kV/mm}$ ) in order to avoid arcing in air ambient. Figure 16 presents an example of diode forward  $I(V)$  characteristics measured at different temperatures before and after the secondary passivation. It is observed that the latter did not affect the functionality

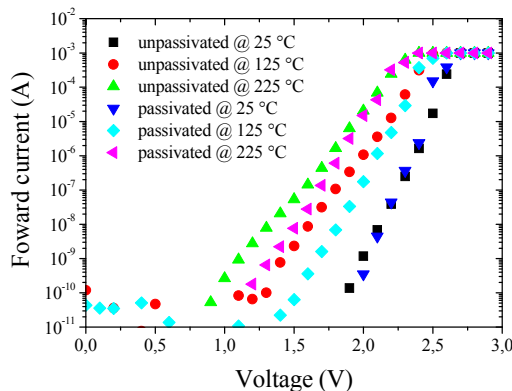


**Figure 16.** Forward current *vs.* voltage characteristics at three different temperatures before and after the BPDA-PDA passivation realization. The current was limited at  $1 \text{ mA}$ . The diode  $P^+$ -emitter diameter and JTE length are  $400 \text{ }\mu\text{m}$  and  $500 \text{ }\mu\text{m}$ , respectively. Characterizations were performed in vacuum.

of the component. On the contrary, an improvement of the diode ideality factors at low forward current levels resulted compared to the non coated diode ones, especially at higher temperatures. A positive effect could be noticed on the reverse  $I(V)$  curves up to -600 V applied voltage as well (not shown here).

The typical high voltage reverse characteristics measured at ambient temperature for the selected best diodes are shown on Figure 17a. The breakdown event always occurred suddenly, at a voltage value between 5 kV and 6 kV, and leaving a visible mark on the sample located relatively far from the tested component (at a distance longer than 1 mm) as presented on Figure 17b.

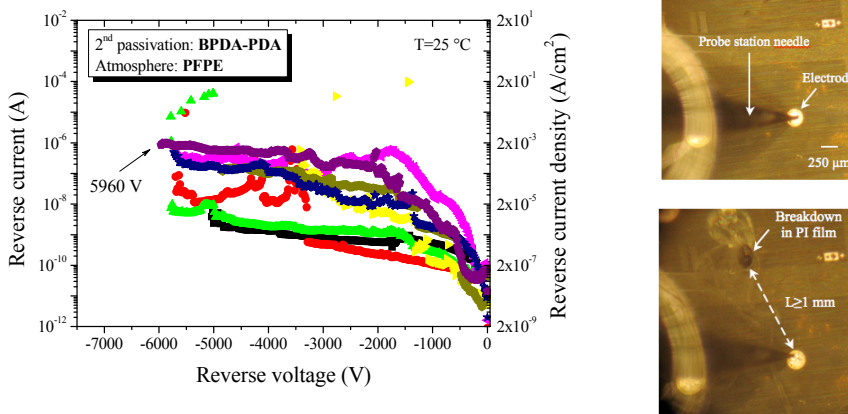


**Figure 17.** (a) Typical reverse characteristics of low leakage diodes passivated with BPDA-PDA (measurements performed in PFPE environment at 25 °C). (b) Views of the same probed diode in PFPE oil, before (top image) and after (bottom image) high voltage measurements.

The tested diodes were not destroyed after the first high voltage measurement, exhibiting approximately the same breakdown voltage values when polarized again several times. Considering the reverse voltage values achieved and the distance observed between the resulting crater and the device, the second passivation layer is certainly at the origin of the failure (the PFPE environment being able to withstand around three times higher voltages), due to the presence of local defects. For another diode, probably situated in a better quality area, a maximal breakdown voltage was measured with a value of 7.3 kV, with a  $I(V)$  characteristics presenting a current knee before breakdown, as can be seen on Figure 18a. Such a breakdown voltage value is very close to the theoretical maximal value assuming an avalanche breakdown in the SiC tested structure. Such a SiC avalanche mechanism in this particular case was further supported by the observation of the post-breakdown degraded zone, situated at the diode itself, the latter being totally destroyed as exhibited on Figure 18b.

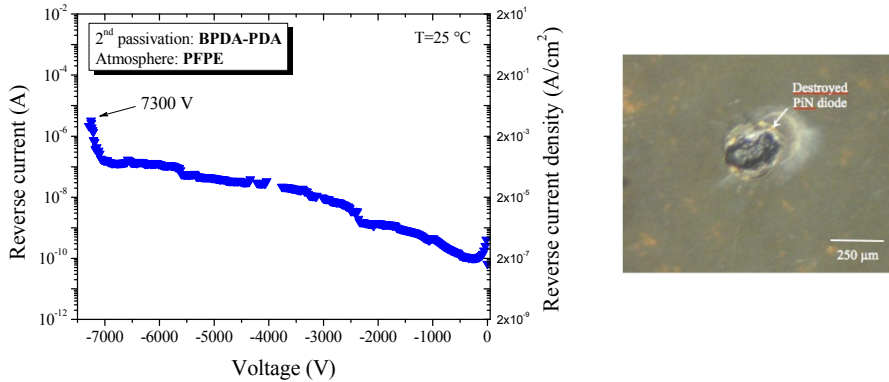


**Figure 18.** (a) Reverse characteristic of a BPDA/PDA passivated diode with the maximal breakdown voltage obtained (performed in PFPE environment at 25 °C). (b) View of the destroyed diode in PFPE oil after the high voltage measurement.

So the feasibility and the potentiality of the BPDA-PDA films for high voltage SiC device secondary passivation could be experimentally demonstrated, positively affecting the current voltage characteristics and allowing high breakdown voltage typical values with a maximum value close to the theoretical limit to be reached. Moreover, a significant improvement in the BPDA-PDA protection efficiency should result from a fabrication entirely performed in clean room conditions and from the use of thicker PI layers.

## 6. Conclusion

This chapter deals with polyimide materials (PIs), having in mind the emerging high temperature semiconductor devices currently demanded for high temperature and high power electronics. Among several PIs already well known for their best thermal properties, very good dielectric characteristics, chemical and radiation resistance, and easy processability, this chapter focuses on BPDA-PDA polyimide, evaluating its superiority for semiconductor insulating coating in the temperature range up to 400 °C.

It is shown that the BPDA-PDA's CTE, which is the closest to the semiconductors (as SiC and GaN) ones, is not the only advantage of this material with regards to the targeted application. In fact, though exhibiting comparable  $T_g$  and  $T_d$  to PMDA-ODA and PPDA-ODA ones in particular, BPDA-PDA on silicon substrate demonstrates a higher properties stability under thermo-oxidative ambient aging than its counterparts, thanks to its chemical nature exempt of C-O-C ether bonds. Indeed, the presented results highlight the insulation long term reliability at 300 °C in air, and at 360 °C in nitrogen ambient, of BPDA-PDA films on semiconductor (no chemical and no electrical degradations having been evidenced up to 5000 h of aging).

The presence of impurities (source of free charges) within the PI films playing a major role in the degradation of their dielectric characteristics above 200 °C, the highest degree of

imidization has to be looked for, as considered in this chapter. An imidization cure (400 °C-temperature, 1 h-duration) is found optimal for maximizing both the low field resistivity and the dielectric strength, in correlation with FTIR spectrometry analysis. Because of its impact on the intrinsic free charges density as well, the film thickness parameter is also taken into account. Its strong influence on the high temperature dielectric properties is underlined, which can not be solved by a higher temperature or longer curing (leading to desimidization). As an example, at 350 °C, the mean dielectric strength of a 8.6 µm-thick film is measured two fold lower than that of a 1.5 µm-thick layer; however it is remaining as high as 2 MV/cm, so comparable to SiC critical field.

Going up to the application, the chapter finally describes an experiment demonstrating the feasibility of the secondary passivation of 7.8 kV SiC bipolar diodes, using BPDA-PDA. The PI coating and etching processes are detailed, resulting in a 4 µm-thick PI layer. The electrical characterization results arise that the applied final fabrication step positively affected the high temperature forward I(V) curves of the diodes. In reverse bias, the typical breakdown voltage, of around 70% of the theoretical maximum value, could be attributed to the presence of local defects throughout the PI coating. So, such a first experiment already attests the potentiality of BPDA-PDA for high voltage secondary passivation, knowing that one can expect an even higher protection efficiency using clean room elaboration conditions, and thicker PI layers.

## Author details

S. Diaham, M.-L. Locatelli and R. Khazaka

*University of Toulouse – UPS – INPT – LAPLACE Laboratory– CNRS, Toulouse, France*

## 7. References

- [1] Sroog C E, Endrey A L, Abramo S V, Berr C E, Edwards W M, Olivier K L (1965). *J. Polym. Sci. A Polym. Chem.* 3: 1373.
- [2] Hougham G, Tesero G, Shaw J (1994). *Macromolecules* 27: 3642-3649.
- [3] Gosh M K, Mittal K L (1996). *Polyimides, Fundamentals and Applications*. New-York: Mercel-Dekker.
- [4] Wayne Johnson R, Wang C, Liu Y, Scofield J D (2007). *IEEE Trans. Elec. Pack. Manuf.* 30: 182-193.
- [5] Ree M, Swanson S, Volksen W (1994). *Polymer*. 34: 1423-1430.
- [6] Ree M, Kim K, Woo S H, Chang H (1997). *J. Appl. Phys.* 81: 698-708.
- [7] Chung H S, Lee C K, Joe Y I, Han H S (1998). *J. Kor. Inst. Chem. Eng. (Hwahak Konghak)*. 36: 329-335 (in Korean language).
- [8] Chung H, Lee C, Han H (2001). *Polymer*. 42: 319-328.
- [9] Cho K, Lee D, Lee M S, Park C E (1997). *Polymer*. 38: 1615-1623.
- [10] Poon T W, Silverman B D, Saraf R F, Rossi A R, Ho P S (1992). *Phys. Rev. B*. 46: 11456-11462.

- [11] Numata S, Oohara S, Fujisaki K, Imaizumi J, Kinjo N (1986). *J. Appl. Polym. Sci.* 31: 101-110.
- [12] Liou H C, Ho P S, Stierman R (1999). *Thin Solid Films.* 339: 68-73.
- [13] Ree M, Shin T J, Lee S W (2001). *Kor. Polym. J.* 9: 1-19.
- [14] Maier G (2001). *Prog. Polym. Sci.* 26: 3-65.
- [15] Tsukiji M, Bitoh W, Enomoto J (1990). *Proc. Inter. Symp. Elec. Insul.* 88.
- [16] Hsaio S H, Chen Y J (2002). *Eur. Polym. J.* 38: 815.
- [17] Pramoda K P, Liu S, Chung T S (2002). *Macromol. Mater. Eng.* 287: 931.
- [18] Ree M, Chu C W, Goldberg M J (1994). *J. Appl. Phys.* 75: 1410.
- [19] Shin T J, Ree M (2007). *J. Phys. Chem. B.* 111: 13894.
- [20] Lee S A, Yamashita T, Horie K, Kozawa T (1997). *J. Phys. Chem. B.* 101: 4520.
- [21] Sung J, Kim D, Whang C N, Oh-e M, Yokoyama H (2004). *J. Phys. Chem. B.* 108: 10991.
- [22] Factor B J, Russell T P, Toney M F (1991). *Phys. Rev. Lett.* 66: 1181.
- [23] Sasaki T, Moriuchi H, Yano S, Yokota R (2005). *Polymer.* 46: 6968.
- [24] Diahm S, Locatelli M L, Lebey T, Malec D (2011). *Thin Solid Films.* 519: 1851-1856.
- [25] Sroog C E (1991). *Prog. Polym. Sci.* 16: 561.
- [26] Chen K M, Wang T H, King J S, Hung A (1993). *J. Appl. Polym. Sci.* 48: 291.
- [27] Hsu T C J, Liu Z L (1992). *J. Appl. Polym. Sci.* 46: 1821.
- [28] Ishida H, Wellinghoff S T, Baer E, Koenig J L (1980). *Macromolecules.* 13: 826.
- [29] Thomson B, Park Y, Painter P C, Snyder R W (1989). *Macromolecules.* 22: 4159.
- [30] Synder R W, Thompson B, Bartges B, Czerniawski D, Painter P C (1989). *Macromolecules.* 22: 4166.
- [31] Pryde C A (1993). *J. Polym. Sci. A: Polym. Chem.* 31: 1045.
- [32] Karamancheva I, Stefov V, Soptrajanov B, Danev G, Spasova E, Assa J (1999). *Vibr. Spectr.* 19: 369.
- [33] Spassova E (2003). *Vacuum.* 70: 551.
- [34] Deligöz H, Yalcinyuva T, Özgümüş S, Yildirim S (2006). *Eur. Polym. J.* 42: 1370.
- [35] Saeed M B, Zhan M S (2006). *Eur. Polym. J.* 42: 1844.
- [36] Anthamatten M, Letts S A, Day K, Cook R C, Gies A P, Hamilton T P, Nonidez W K (2004). *J. Polym. Sci. A: Polym. Chem.* 42: 5999.
- [37] Hietpas G D, Allara D L (1998). *J. Polym. Sci. B Polym. Phys.* 36: 1247.
- [38] Ito Y, Hikita M, Kimura T, Mizutani T (1990). *Jpn. J. Appl. Phys.* 29: 1128.
- [39] Ruggles-Wrenn M B, Broeckert J L (2009). *J. Appl. Polym. Sci.* 111: 228-236.
- [40] Schoeppner G A, Tandon G P, Ripberger E R (2007). *Composites: Part A.* 38: 890-904.
- [41] Tandon G P, Pochiraju K V, Schoeppner G A (2008). *Mater. Sci. Eng. A.* 498: 150-161.
- [42] Meador M A B, Johnston C J, Cavano P J, Frimer A A (1997). *Macromolecules.* 30: 3215-3223.
- [43] Meador M A B, Johnston C J, Frimer A A, Gilinsky-Sharon P (1999). *Macromolecules.* 32: 5532-5538.
- [44] Tsukiji M, Bitoh W, Enomoto J (1990). *Proc. IEEE Int. Symp Elec. Insul.* pp. 88-91.
- [45] Li L, Bowler N, Hondred P R, Kessler M R (2011). *J. Phys. Chem. Solids.* 72: 875-881.
- [46] Dine-Hart R A, Parker D B V, Wright W W (1971). *Br. Polym. J.* 3: 222-236.

- [47] Diaham S, Locatelli M L, Lebey T, Raynaud C, Lazar M, Vang H, Planson D (2009). *Mater. Sci. Forum.* 615-617: 695-698.
- [48] Lazar M, Raynaud C, Planson D, Chante J-P, Locatelli M-L, Ottaviani L, Godignon P (2003). *J. Appl. Phys.* 94: 2992-2999.
- [49] Konstantinov A O, Wahah Q, Nordell N, Lindefelt U (1997). *Appl. Phys. Lett.* 71: 90-92.